JLB

Article

Adipose tissue macrophages develop from bone marrow–independent progenitors in *Xenopus laevis* and mouse

Syed F. Hassnain Waqas,[*,1] Anna Noble,[†,1] Anh C. Hoang,[*] Grace Ampem,[*] Manuela Popp,[*] Sarah Strauß,[‡] Matthew Guille,[†] and Tamás Röszer*[*,2]*

[*]Institute of Comparative Molecular Endocrinology, University of Ulm, Ulm, Germany; [†]European *Xenopus* Resource Centre, School of Biological Sciences, University of Portsmouth, Portsmouth, United Kingdom; and [‡]Ambystoma Mexicanum Bioregeneration Center, Department of Plastic, Aesthetic, Hand and Reconstructive Surgery, Hannover Medical School, Medizinische Hochschule Hannover, Hannover, Germany

RECEIVED MARCH 2, 2017; REVISED MAY 26, 2017; ACCEPTED MAY 27, 2017. DOI: 10.1189/jlb.1A0317-082RR

ABSTRACT

ATMs have a metabolic impact in mammals as they contribute to metabolically harmful AT inflammation. The control of the ATM number may have therapeutic potential; however, information on ATM ontogeny is scarce. Whereas it is thought that ATMs develop from circulating monocytes, various tissue-resident Mϕs are capable of self-renewal and develop from BM-independent progenitors without a monocyte intermediate. Here, we show that amphibian AT contains self-renewing ATMs that populate the AT before the establishment of BM hematopoiesis. *Xenopus* ATMs develop from progenitors of aVBI. In the mouse, a significant amount of ATM develops from the yolk sac, the mammalian equivalent of aVBI. In summary, this study provides evidence for a prenatal origin of ATMs and shows that the study of amphibian ATMs can enhance the understanding of the role of the prenatal environment in ATM development.
***J. Leukoc. Biol.* 102: 845–855; 2017.**

Introduction

ATMs are resident Mϕs of AT in mammals [1] and have a largely unexplored role in AT immunity [2] but a better understood impact on metabolism [1]. ATMs can support normal AT function, but can also trigger AT inflammation and IR and can correspondingly contribute to the development of obesity comorbidities [1–4]. Because ATMs are associated with the rising prevalence of obesity and its comorbidities [1, 3–5], they are of great pathophysiologic relevance.

The quantity and the so-called activation state of ATMs are the 2 main determinants of their metabolic effects [1, 2]. Obesity increases the number of ATMs as a result of increased monocyte infiltration and local ATM proliferation in AT [1, 6, 7]. The increase in ATM content in obesity is associated with an inflammatory ATM phenotype, which is the result of classic or M1 Mϕ activation [1, 2]. M1 activation of ATMs is promoted by modified lipids, lipoproteins, and cytokines of the obese AT. M1 ATMs exacerbate AT inflammation, which can lead to IR [1–4]. In contrast, lean AT is rich in alternatively activated, so-called M2 ATMs, which are thought to support homeostatic AT functions [1]. Inhibition of M1 activation and maintenance of a metabolically healthy M2-dominant ATM population is a therapeutic strategy for treating obesity and IR [1, 2, 8]. Whether ATMs of lean AT develop from blood monocytes or are replenished by local proliferation of ATMs is unknown [2]. Because Mϕs are present in almost all organs, pharmacologic manipulation of Mϕ activation and proliferation can have beneficial effects in AT; however, detrimental effects have been observed in other tissues. To avoid such off-target effects, recent research efforts have focused on the identification of developmental programs and marker proteins that are specific for individual tissue-resident Mϕs [9–12]. Such an approach could allow for targeted manipulation—for example, drug delivery to specific Mϕ niches. Therefore, a better understanding of the ontogeny of ATMs can help to develop methods to specifically increase the production of M2 ATMs without affecting other tissue-resident Mϕs. Nevertheless, in contrast to other tissue-resident Mϕs, such as microglia, Kupffer cells, or osteoclasts, to

Abbreviations: ACP = acid phosphatase, AT = adipose tissue, ATM = adipose tissue Mϕ, aVBI = anterior ventral blood island, BAT = brown adipose tissue, BM = bone marrow, IR = insulin resistance, iWAT = inguinal white adipose tissue, KO = knockout, NPFF = neuropeptide FF, PFA = paraformaldehyde, pI:pC = polyinosine polycytidylic acid, SC = stromal cell, TEM = transmission electron microscopy, WAT = white adipose tissue, YS = yolk sac

The online version of this paper, found at www.jleukbio.org, includes supplemental information.

1. These authors contributed equally to this work.
2. Correspondence: Institute of Comparative Molecular Endocrinology, Center of Biomedical Research, University of Ulm, Science Park I, 89081 Helmholtz-Strasse 8/1, Ulm, BW 89081, Germany. E-mail: tamas.roeszer@uni-ulm.de; Twitter: https://twitter.com/uni_ulm

This is an Open Access article distributed under the terms of the Creative Commons Attribution-NonCommercial 4.0 International (CC BY-NC 4.0) (http://creativecommons.org/licenses/by-nc/4.0/) which permits noncommercial use, distribution, and reproduction in any medium, provided the original work is properly cited.

date little is known about the developmental program of ATMs [2].

Comparative studies have facilitated the understanding of the development of specific cell types and may provide evidence of the evolutionary origin of ATMs. In this study, we show that ATMs are present in the African clawed frog *Xenopus laevis*, a widely used model of vertebrate development. *Xenopus* ATMs develop from progenitors of the extraembryonic aVBI and have the ability to proliferate. aVBI is the equivalent of the hematopoietic tissue of the mammalian YS. Accordingly, we found that YS Mϕs give rise to ATMs in the mouse.

MATERIALS AND METHODS

X. laevis and *Ambystoma mexicanum* strains

For assays on adult *X. laevis* fat bodies, we used specimens from wild-type female frogs and *lurp*:eGFP [*Xla.Tg(slurp1l:GFP)*^{1Mohun}] or *sct*:eGFP (European *Xenopus* Resource Centre, Portsmouth, United Kingdom) transgenic frogs at age 1–2 yr. Animals were maintained according to previously described general protocols [13]. For developmental studies, *lurp*:eGFP embryos were cultured and staged as described previously [13, 14]. Fat body specimens of *A. mexicanum* were obtained from wild-type adult females (Internal MHH file reference: 2012/2, donor animals according §4 TierSchG) that were bred and housed at the Ambystoma Mexicanum Bioregeneration Center (Hannover, Germany), as previously described [15].

Manipulation of *X. laevis* embryos

All animal work at the European *Xenopus* Resource Centre was approved by the Animal Welfare Ethical Review Body of the University of Portsmouth and carried out under the appropriate Home Office license. *X. laevis* were obtained from the European *Xenopus* Resource Centre, maintained at 18°C on a daily light/dark cycle for 13–11 h, and fed daily with Horizon XP pellets. Wild-type *X. laevis* eggs were obtained by injecting 400 IU of human chorionic gonadotrophin into dorsal lymph sacs of adult females on the evening before egg collection. Eggs were fertilized in vitro with macerated testes, dejellied with 2% cysteine hydrochloride (pH 7.8–8.0), and cultured in 0.1× modified Barth's solution. Staging of *X. laevis* embryos was performed according to Nieuwkoop and Faber [14]. Cas9 mRNA (2 ng/embryo) and sgRNA (each 400 pg/embryo) were injected into the animal pole of 1-cell stage embryos [16].

Generation of Cas9 mRNA and gRNAs

Cas9 mRNA and sgRNA were generated as described [17]. Oligonucleotides used to prepare sgRNA templates are listed in Supplemental Table 2. We used the online tool Crispr (http://www.crisprscan.org/) to design the 5′-oligonucleotides of sgRNAs. For sgRNA transcription, DNA templates were obtained by PCR assembly (forward primer: Supplemental Table 4; and reverse primer: 5′-AAAAGCACCGACTCGGTGCCACTTTTTCAA-GTTGAT-AACGGACTAGCCTTATTTTAACTTGCTATTTCTAGCTCTAAAAC-3′). Amplicons were transcribed with the MEGAshortscript T7 Transcription Kit (Thermo Fisher Scientific, Waltham, MA, USA) followed by DNase digestion, and transcripts were purified with SigmaSpin Sequencing Reaction Clean-Up columns (Sigma-Aldrich, St. Louis, MO, USA). Cas9 mRNA was produced by using the mMessage mMachine Kit SP6 (Thermo Fisher Scientific Life Sciences) from a modified Cas9 construct in pCS2 (Supplemental Fig. 6).

Evaluation of gene targeting efficiency in sgRNA/Cas9-injected *X. laevis* embryos

Targeting efficiency was examined at stage 32. We randomly collected 5 healthy embryos from each injection, extracted genomic DNA by using the DNeasy Blood and Tissue Kit (Qiagen, Hilden, Germany), and amplified the targeted region by PCR (for primers, see Supplemental Table 3). We performed a standard T7 endonuclease I assay to detect Cas9-induced mutations.

Detection of YS-derived ATMs in mouse

To label YS-derived Mϕs, we adapted the lineage-tracing protocol described elsewhere [11, 18]. In brief, we crossed the Cx3cr1$^{tm21.(cre/ERT2)Jung}$ (The Jackson Laboratory, Bar Harbor, ME, USA) mouse line, which carries a tamoxifen inducible Cre recombinase under the control of the Cx3cr1 promoter, with the Gt(ROSA)26Sor tm1$^{(CAG-tdTomato-EGFP*)Etes}$ (The Jackson Laboratory) reporter line. The latter mouse line expresses red fluorescent Tomato protein, along with a stop codon–blocked eGFP sequence. When Cre recombinase is active, the sequence that encodes red fluorescent Tomato protein is excised, along with the stop codon that blocks eGFP expression. As a result, cells with an active Cx3cr1 promoter at the time of tamoxifen injection will express eGFP, whereas other cells maintain the expression of the red fluorescent Tomato protein. To avoid contamination with maternal Mϕs, we used mothers that lacked Cre recombinase, and, thus, maternal Mϕs remained fluorescent red. Both mouse lines were kindly provided by Dr. Bernd Baumann and Prof. Dr. Jan Tuckermann (University of Ulm, Ulm, Germany).

To measure ATM proliferation and to characterize CX_3CR1^+ ATMs, we used C57/BL6 male mice at age postnatal d 7 and 56 (The Jackson Laboratory). All mouse strains were kept under specific pathogen–free conditions, and experiments were carried out according to local legislation.

Organ imaging, histology, and electron microscopy

Dissected fat bodies and developing tadpoles were photographed with a Nikon digital camera (Nikon, Tokyo, Japan) assembled onto a white lightbox. For hematoxylin and eosin staining and ACP and peroxidase enzyme histochemistry, fat body samples were fixed in 4% PFA in PBS for 24 h, paraffin embedded, sectioned, and stained as described [19, 20] For TEM, fat body specimens, pancreas, or cells that were isolated from the fat body were fixed in a 4:1 mixture of 4% PFA and concentrated glutaraldehyde and processed as previously described [19]. For imaging *lurp*:eGFP$^+$ and *sct*:eGFP$^+$ cells, fat bodies, spleen, and liver of tadpoles or adult specimens were cryosectioned. In brief, tissues were fixed in 4% PFA overnight, immersed in a 10% sucrose solution in PBS overnight, embedded, frozen in Surgipath embedding medium (Leica Biosystems, Wetzlar, Germany), and sectioned by using a Leica cryostat (Leica Biosystems) at 7–10 μm thickness. The eGFP signal was photographed with a Leica fluorescent microscope using DAPI as a counterstain in Vectashield Mounting Medium (Vector Laboratories, Burlingame, CA, USA).

For immunostaining of NPFF, we used cryosections and a primary Ab from Abcam (Cambridge, United Kingdom). Transmitter vesicles were labeled with an Ab raised against synaptic vesicle protein 2 (Developmental Studies Hybridoma Bank, Iowa City, IA, USA). Nonspecific binding of primary Abs was reduced by preincubating cryosections with 1% normal goat serum for 2 h. Sections were incubated with primary Abs overnight. This was followed by a 2-h incubation with fluorescent secondary Abs and counterstaining with DAPI-containing Vectashield. CX3CR1 was detected on cryosections of mouse WAT by using an Ab from Abcam (Supplemental Table 4). Cell contours were labeled with fluorescent phalloidin (Sigma-Aldrich).

To assess BM development, we used developing hindlimbs of tadpoles and developed femurs of adult frogs. Organs were fixed with 4% PFA overnight. Mineralized adult femurs were decalcified with 10% EDTA at 37°C. Specimens were embedded in paraffin and processed for sectioning, followed by hematoxylin and eosin or ACP staining.

Isolation of SCs of the *Xenopus* fat body

SCs of *Xenopus* fat body specimens were separated from adipocytes by using collagenase digestion as previously described for ATM isolation from mouse fat depots [21]. Adipocytes were used for RNA extraction. ATMs were suspended in selection medium that consisted of 2 mM EDTA and 0.5% BSA in PBS, pH 7.4. Cell density was adjusted to 10^6 cells/ml and analysis was performed on a Becton Dickinson LSR II Cytometer (BD Biosciences, Franklin Lakes, NJ, USA). Size and intracellular complexity was assessed by using FSC-A and SSC-A parameters of cell populations. Identified cell populations—RBCs, ATMs, lymphocyte-like cells—were retrieved with preparative cell sorting by using a FACS Aria Cell sorter (BD Biosciences). Sorted cells were collected for additional analysis by

TEM or RNA extraction. ATMs were also collected for additional in vitro culture as described below. Results of FACS analyses have been deposited in the Flow Repository to allow secondary use.

In vitro culture of *Xenopus* ATMs

ATMs were suspended in FACS selection medium that consisted of 2 mM EDTA and 0.5% BSA in PBS (pH 7.4) and were allowed to adhere to 6-well plates in RPMI 1640 medium with 10% heat-inactivated FCS. Cells were maintained at 23°C in sterile cell culture hoods under 5% CO_2.

To measure phagocytosis activity, fluorescently labeled latex beads or nonconjugated latex beads (Sigma-Aldrich) were added to cultures at a ratio of 1:5 Mϕ:latex bead and incubated at 23°C for 4 h. Mϕs were harvested by trypsinization, washed with FACS selection medium, and processed for FACS analysis. To detect the phagocytosed beads by microscopy, we cultured Mϕs on glass-bottom culture plates (Cell View slides; Greiner Bio-One, Frickenhausen, Germany). For negative control, we used ATMs without added beads. After the phagocytosis assay, ATMs were fixed with 4% PFA for 20 min, nuclei were stained with DAPI-containing Vectashield, and analysis was carried out by using a Leica fluorescent microscope. Using the same Leica microscope, we captured image sequences of the phagocytosis process in living ATM cultures by using a differential interference contrast objective.

For the activation of ATMs, cultures were treated with PBS as vehicle or with 100 ng/ml LPS from *Escherichia coli* or 5 μg/ml pI:pC (both from Sigma-Aldrich) or with 1 nM synthetic NPFF (Phoenix Pharmaceuticals, Burlingame, CA, USA).

To assay colony formation of fat body SCs, we used a soft agar colony-forming assay for *Xenopus* hematopoietic colonies as previously described [22]. In brief, cells were suspended in 0.5% agarose dissolved in DMEM and were seeded on the surface of a 1% agarose layer made with DMEM. Semisolid agarose layers were covered with DMEM and incubated at 23°C in sterile cell culture hoods under 5% CO_2. Colonies were collected for TEM or were photographed in situ by using a wide-field Leica microscope with a differential interference contrast objective.

To measure proliferation, SCs were cultured with 0.1 mg/ml BrdU (Sigma-Aldrich) for various durations in 6-well culture dishes. Cells were collected for FACS analysis by trypsinization and fixed with 4% PFA for 20 min, then incorporated BrdU was detected with a PE-conjugated anti-BrdU Ab (BU20A; eBioscience, San Diego, CA, USA). For negative control, we used vehicle-treated cells and BrdU-pulsed cells that were incubated with isotype controls.

Isolation and FACS analysis of mouse ATMs

We collected epididymal WAT from adult (postnatal day 56) C57/BL6 mice. Tissues were pooled from 3–5 animals and ATMs were isolated by using collagenase digestion as previously described [21]. The same technique was used to isolated SCs and ATMs from BAT and iWAT of mice at postnatal day 7 or 56. In the case of young mice (postnatal day 7), we pooled tissue samples from 12–18 animals. Cell density was adjusted to 10^6 cells/ml in selection medium—the same as that used for the analysis of *Xenopus* ATMs—and analysis was performed on a BD LSR II Cytometer (BD Biosciences). Staining was performed after fixing cells with 4% PFA for 20 min. We incubated cells with Fc-blocker Ab, followed by fluorescent Abs or with matching isotype controls for 2 h, as previously described [19]. After a 2-h incubation, cells were washed in selection buffer and used for analysis. Abs used are listed in Supplemental Table 4.

RNA extraction and quantitative PCR

Total RNA was isolated with TRI reagent (Sigma-Aldrich). Integrity of the RNA was evaluated by denaturing agarose gel electrophoresis. Only non-degraded RNA samples were used for cDNA synthesis, as previously described [23]. We used the Viia7 qPCR platform (Thermo Fischer Scientific) for analysis, and gene expression values were expressed as relative mRNA level on the basis of the δCT and δδCT methods, using *Bactin* and *Ppia/Cypa* as reference genes for mouse, and *bactin* and *gapdh* as reference genes for *Xenopus*. Primer sequences are provided in Supplemental Table 5.

Whole-body irradiation and BM chimerism in mouse

As recipients, we used 8- to 10-wk-old $CD45.1^+$ C57BL/6 mice (The Jackson Laboratory). Mice were placed in a restrainer to ensure immobility during γ-irradiation. We applied a 10.5-Gy single dose of irradiation. Donor BM from CD45.2 allele-bearing C57BL/6 mice (The Jackson Laboratory) was harvested by flushing the femur BM under sterile conditions, and lineage-negative $CD45.2^+$ BM cells were i.v. injected at 400×10^3 cells/recipient density. As competitor cells, we injected an equal amount of lineage-negative cells from $CD45.1^+$ BM. The amount of $CD45.1^+$ and $CD45.2^+$ leukocytes in BM and peripheral blood and the amount of $CD45.1^+$, $F4/80^+$, and $CD45.2^+$, $F4/80^+$ ATMs was measured by FACS at 20 wk after BM transplantation.

Statistical analysis

All results are expressed as means ± SEM. The 2-tailed Student's unpaired *t* test or a 1-way ANOVA with Dunnett's post hoc test was used for statistical analysis. A P value < 0.05 was considered significant. Statistical analyses were performed by using the Prism 5 (GraphPad Software, La Jolla, CA, USA).

RESULTS

Visceral AT of *X. laevis* is rich in Mϕs

Amphibians were the first vertebrates to evolve and develop visceral WAT [24]. WAT is present in the abdominal cavity where it forms paired fat bodies (**Fig. 1A**). Whether Mϕs are associated with amphibian WAT is unknown. Histologic assessment of *Xenopus* fat bodies revealed WAT that is rich in SCs (Fig. 1B), with the majority exhibiting strong ACP and peroxidase activity (Fig. 1C). Both enzymes are associated with phagosomes and are expressed by amphibian Mϕs [25, 26]. By using TEM to examine the structure of sorted cells from WAT stroma, we identified cells with the typical morphology of *Xenopus* Mϕs [27] (Fig. 1C, D, and J and Supplemental Fig. 1A–C) and that expressed the Mϕ marker, lurp (Supplemental Fig. 1D). Furthermore, phagocytosis activity was restricted to Mϕs of the WAT stroma (Fig. 1E–H and Supplemental Video 1), which supports the notion that, analogous to mammalian WAT, amphibian WAT is infiltrated by ATMs.

Mϕ activation in amphibians remains poorly understood, and it is not known whether homologous mechanisms of M1 and M2 Mϕ polarization exist [28]; however, it has been reported that a NO-producing, pathogen-killing activation state of *Xenopus* Mϕs can be elicited in vitro by pI:pC and, to a lesser extent, LPS [28], which is reminiscent of the M1 activation of mammalian Mϕs. To assess whether *Xenopus* ATMs can adopt an M1-like activation state, we challenged *Xenopus* ATMs in vitro with either pI:pC for 4 h or LPS for 6 and 18 h and measured the transcription of genes that encode inflammatory mediators and receptors that are known to initiate pathogen clearance in *Xenopus*. These genes include *nos2* and *ifng* (IFN-γ), which are produced by *Xenopus* Mϕs in response to viral and bacterial infection [29, 30], and *mif* (Mϕ inhibitory factor-1), which is linked to the activation of leukocyte migration in *Xenopus* [31]. We found that pI:pC treatment increased *nos2* and *mif* transcription (Supplemental Fig. 1E). Of note, *Xenopus* ATMs were relatively insensitive to LPS treatment, which is in agreement with data from amphibian Mϕs [32]. Accordingly, prolonged (18 h) LPS exposure, but not short-term (6 h) exposure, increased the transcription of *csf1*, *csf1r* (csf-1 receptor), *ifng*, and *mif*, whereas *tgfb* (TGF-β) transcription remained unchanged (Supplemental Fig. 1F). CSF1 may polarize *Xenopus* Mϕs

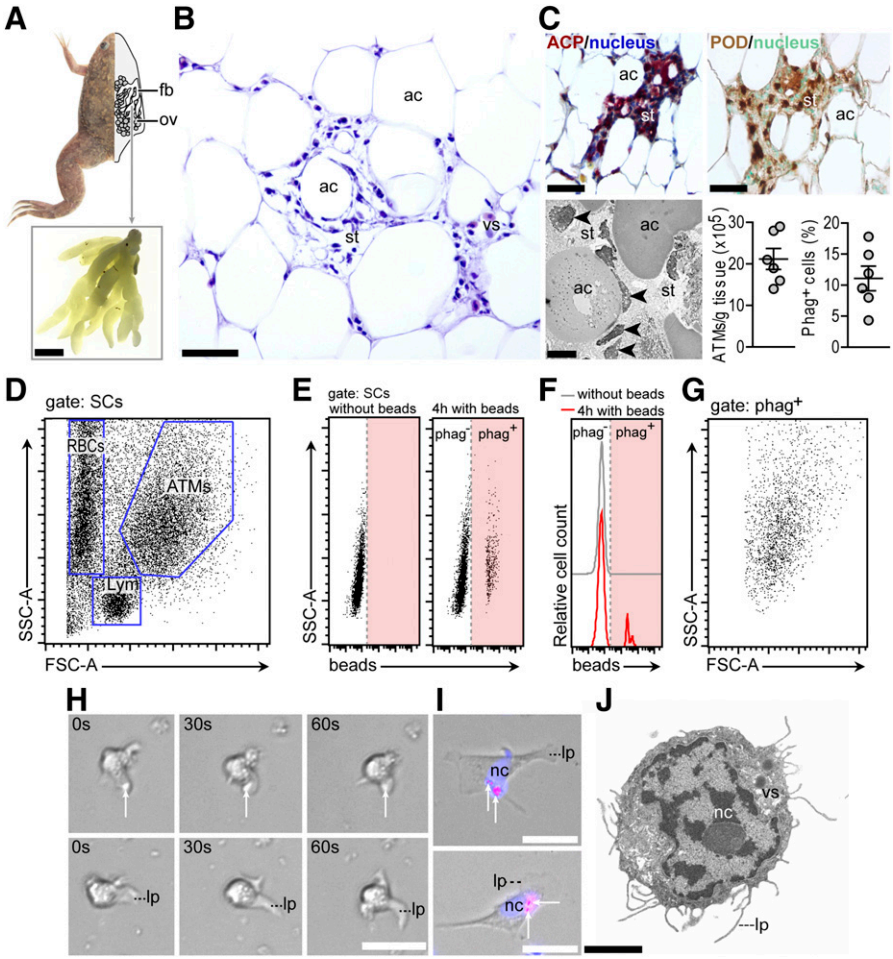

Figure 1. AT Mϕs in *X. laevis*. (A) Anatomy of the visceral fat depot. Scale bar, 1 cm. (B) Histologic assessment of the fat body by hematoxylin and eosin staining. Scale bar, 100 μm. (C) Enzyme histochemistry and ultrastructure of the fat body stroma, and quantification of ATMs. ACP- and peroxidase (POD)-positive cells in the fat body (top). Scale bar, 50 μm. TEM image of the fat body (bottom left). Arrowheads indicate ATMs (leukocytes with abundant endocytic vesicles). Scale bar, 1 μm. ATM content and percentage of phagocytosing (phag$^+$) cells in the stroma (bottom right). The raw data set is available at the Flow Repository under accession number FR-FCM-ZYZF. (D) FACS analysis of SCs. For TEM images of the sorted RBCs, ATMs, and Lym, and for additional details of the FACS analysis, see Supplemental Fig. 1A–D. (E–G) Identification of phagocytosing cells in AT stroma. Isolated SCs were incubated in vitro with fluorescent latex beads for 4 h. (H) Time-lapse sequence of a phagocytosing ATM. The entire time lapse sequence is shown as Supplemental Video 1. Scale bar, 25 μm. (I) ATMs with ingested fluorescent latex beads (arrows). Scale bar, 15 μm. (J) TEM images of ATMs. Scale bar, 1 μm. Additional TEM images of ATMs are shown in Supplemental Fig. 1A. ac = adipocyte, fb = fat body; FSC = forward scatter, lp = lamellipodia, Lym = lymphocytes, nc = nucleus, ov, ovary; phag$^-$ = cells without phagocytosed beads, phag$^+$ = cells with phagocytosed beads, SSC = side scatter, st = stroma, ves = blood vessel, vs = vesicles.

toward a NOS2-expressing, and hence, M1-like, activation state [28]. Although amphibians have TLRs—and notwithstanding that TLR signaling ensures pathogen recognition and activation of the innate immune response—recognition of LPS is weak in amphibians, possibly as a result of the truncated TLR4 [32]. Collectively, the results show that *Xenopus* WAT contains immune-competent ATMs that can adopt an M1-like activation state in response to pathogen-associated signals (Fig. 1 and Supplemental Fig. 1).

Xenopus ATMs can self-renew

In addition to their activation state, increased ATM proliferation contributes to the metabolic dysfunction of obese WAT in mammals [6, 33]. To determine whether *Xenopus* ATMs had proliferative capacity, SCs of WAT were isolated and labeled in vitro with BrdU. We observed that BrdU incorporation was present only in ATMs (**Fig. 2A–C**). Because false-positive staining may occur in phagocytosing cells that engulf BrdU-labeled cells, we confirmed that ATMs were able proliferate by culturing them for 24–72 h in soft agar and monitoring their ability to grow as colonies. As observed by differential interference contrast microscopy, the resulting colonies displayed a morphology that resembled that of *Xenopus* hematopoietic colonies (Fig. 2D) [22], and TEM analysis confirmed leukocyte morphology (Fig. 2E).

Given the ability of *Xenopus* ATMs to proliferate and form colonies, we next asked whether WAT contains hematopoietic progenitors. The expression level of *scl* (stem cell leukemia)—a key transcription factor of amphibian hemangioblast development and hematopoiesis [34, 35]—in SCs of WAT was compared with that in the hematopoietic organs liver, spleen, and BM. Spleen and liver had the highest levels of *scl* transcription in adult *Xenopus* (**Fig. 3A**), whereas BM, which makes only a minor contribution to hematopoiesis in adult amphibians, had negligible expression. SCs of WAT had *scl* levels that were comparable to those of the spleen and liver (Fig. 3A). The presence of scl$^+$ cells in WAT was confirmed by histology and FACS analysis of transgenic *scl*eGFP *Xenopus* fat bodies (Fig. 3B; scl$^+$ cells in spleen and liver are shown in Supplemental Fig. 2).

During amphibian embryogenesis, the first wave of Mϕs develops from lurp$^+$ precursors, which also express *scl* and have the ability to proliferate [34]. Lurp$^+$ myeloid cell precursors occur first in the aVBI in the early tailbud embryo [34], the so-called extraembryonic compartment of hematopoiesis that corresponds to the mammalian YS hematopoietic tissue [36]. aVBI develops into the vitelline veins, which contribute to the formation of the liver sinusoids [36] and, thus, may allow for the colonization of the developing liver with lurp$^+$ cells. Accordingly, we detected *lurp* transcription in the adult liver and spleen (Fig. 3C). In addition, BM displayed a comparable level of *lurp* transcription (Fig. 3C), conceivably as a result of its ability to generate myeloid cells in the *Xenopus* adult [37].

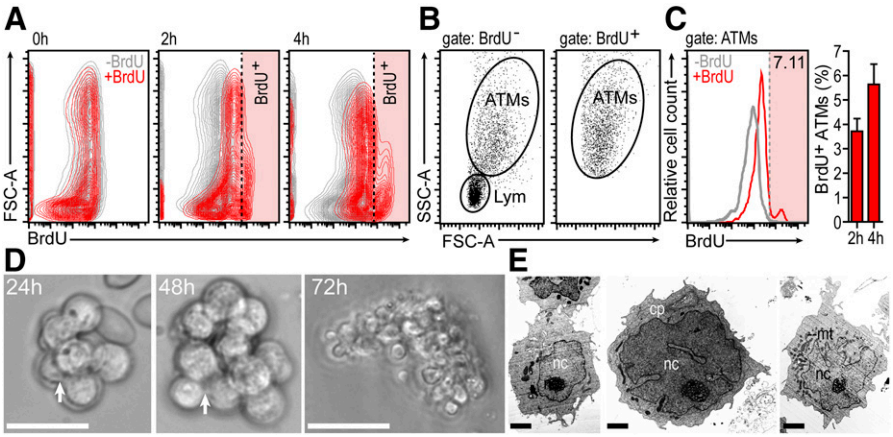

Figure 2. Self-renewal of ATMs in *X. laevis*. (A) Isolated SCs were cultured in vitro and labeled with BrdU (indicated in red; $n = 6$). In the control experiment, cells were incubated with vehicle only (indicated in gray). Presence of BrdU$^+$ cells was detected by FACS. The raw data set is available in the Flow Repository under accession number FR-FCM-ZYZG. (B) Characterization of BrdU$^+$ cells with FACS. (C) Amount of BrdU$^+$ ATMs after 2–4 h of incubation with BrdU. Histogram shows BrdU labeling after 4 h ($n = 3$). (D) SCs were cultured in vitro in soft agar. Colonies formed by SCs were detected after 24, 48, and 72 h. Arrow denotes cell-cell attachment site. Scale bar, 50 μm. (E) TEM images of SC colonies formed in soft agar. Representative images (E1-E3). Scale bar, 0.5 μm. cp = cytoplasm, FSC = forward scatter, Lym = lymphocytes, mt = mitochondria, nc = nucleus, SSC = side scatter.

Whereas it has been shown that lurp$^+$ Mϕ precursors of the aVBI proliferate and infiltrate tissues before the development of the circulatory system [34], it is not known whether they reach WAT. We found that *lurp* transcription was higher in adult SCs of WAT than in tested hematopoietic organs (Fig. 3C), which suggests that it is rich in lurp$^+$ Mϕ progenitors. The presence of lurp$^+$ cells was confirmed in the stroma by FACS analysis of transgenic *lurp*:eGFP *Xenopus* (Fig. 3D and Supplemental Fig. 2) [34]. Expression of *lurp* in the WAT was restricted to the ATM population as shown by FACS analysis (Supplemental Fig. 1D). Collectively, these findings strongly suggest that *X. laevis* fat bodies contain a self-renewing population of ATMs.

Xenopus ATMs settle in WAT before the development of BM

We next investigated the stage in ontogeny at which ATMs emerge in WAT. We detected fat bodies in *Xenopus* embryos from stage 60 onwards (Supplemental Fig. 3A), a period during which

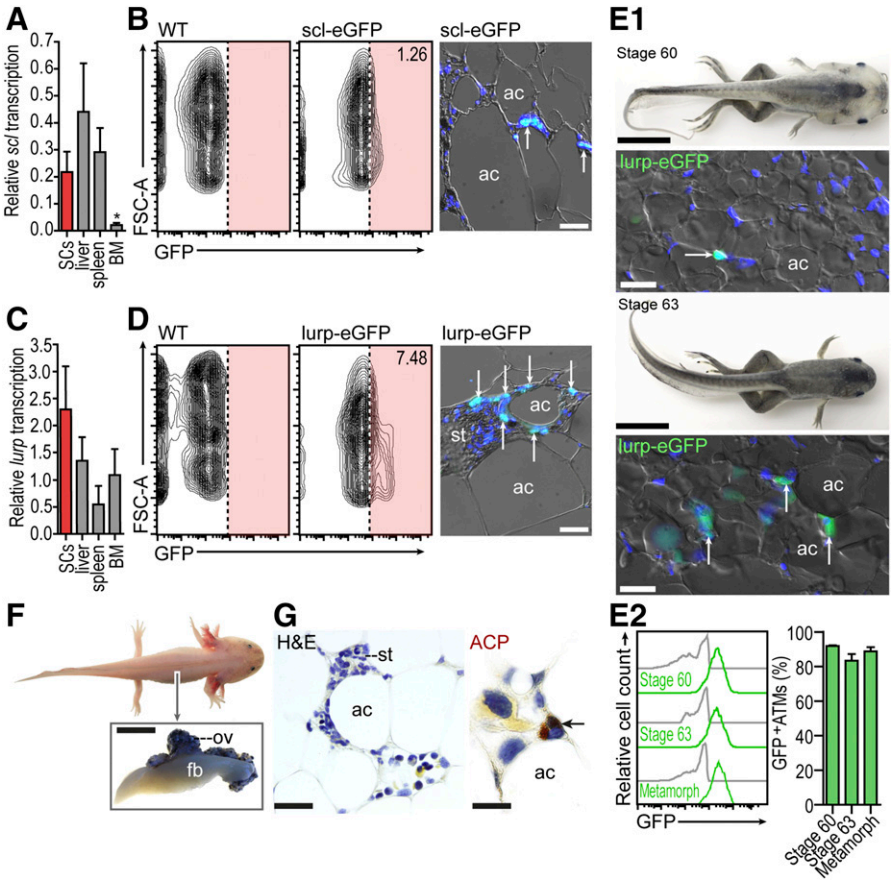

Figure 3. Development of ATMs in *X. laevis*. (A) Relative transcription of the hematopoietic marker *scl* in SCs of the fat bodies and in various hematopoietic tissues ($n = 6$; $^*P < 0.05$, Student's 2-tailed, unpaired t test). (B) Analysis of *scl*:eGFP$^+$ cells in adult fat bodies using FACS and histology ($n = 3$). Arrows show *scl*:eGFP$^+$ cells. Scale bar, 50 μm. Additional details are shown in Supplemental Fig. 2. (C) Relative transcription of the Mϕ precursor marker, *lurp*, in SCs of the adult fat bodies and in various hematopoietic tissues ($n = 6$). (D) Analysis of *lurp*:eGFP$^+$ cells in adult fat bodies using FACS and histology ($n = 3$). Arrows show *lurp*:eGFP$^+$ cells. Scale bar, 50 μm. Additional details are shown in Supplemental Fig. 2. (E1) Presence of *lurp*:eGFP$^+$ cells in developing fat bodies. Arrows show *lurp*:eGFP$^+$ cells. Scale bars, 1 cm (in macroscopic images showing developing tadpoles) and 50 μm (for the histology images). (E2) FACS analysis of *lurp*:eGFP$^+$ ATMs at various developmental stages ($n = 5$ each stage). The data set is available in the Flow Repository under accession number FR-FCM-ZYZE. (F) Anatomy of the fat body in *A. mexicanum*. Scale bar, 1 cm. (G) Hematoxylin and eosin (H&E)–stained section and ACP enzyme histochemistry of the fat body. Arrow shows an ACP$^+$ cell. Scale bar, 50 μm. ac = adipocyte, fb = fat body, FSC = forward scatter, st = stroma, ov = ovary.

hematopoiesis takes place in the liver and kidney. Lurp$^+$ ATMs were also detected from stage 60 (Fig. 3E). Infiltration of WAT by lurp$^+$ ATMs was concomitant with the development of BM-independent hematopoiesis. Indeed, WAT and ATM development preceded the development of BM (Supplemental Fig. 3A and B). Although BM of *Xenopus* can generate leukocytes [37], ACP$^+$ BM Mϕs were detected only in adults, where Mϕs were associated with fat cells (Supplemental Fig. 3C).

As a robust test to determine whether ATMs could be generated in the complete absence of BM hematopoiesis, we took advantage of the fact that the axolotl, *A. mexicanum*, lacks BM hematopoietic progenitors [38]. Liver and spleen are responsible for definitive hematopoiesis in the axolotl in place of BM [38]. In axolotl WAT, we identified ACP$^+$ ATMs (Fig. 3F and G), which indicates that hepatic and splenic hematopoiesis could generate ATMs. Collectively, these findings show that amphibian WAT is colonized by BM-independent Mϕ precursors and that ATMs exist despite the complete lack of BM hematopoiesis.

Xenopus and mouse share a homologous mechanism of ATM development

Xenopus embryonic development shares many features with mammalian embryogenesis. The functional equivalent of aVBI in mammals and birds is YS [36], and YS-derived Mϕs give rise to tissue-resident Mϕs in birds [39]. Moreover, it has been recently shown that YS-derived Mϕ progenitors contribute to various tissue-resident Mϕ populations in the mouse, such as microglia, cardiac-resident Mϕs, and arterial Mϕs [10, 11, 18, 40]. In mammals, the first wave of YS Mϕs has a maternal origin, and these cells persist between embryonic day 7.5 and 9.5. From embryonic day 8, YS produces a second wave of Mϕs that is characterized by 4 developmental stages with specific cell-surface expression of antigens (Supplemental Table 1). We found that ATMs of the adult mouse WAT share similarities in cell-surface pattern with YS Mϕs, such as their CD45$^+$, Kit^{low}, F4/80$^+$, MCSFR(CD115)$^+$, and CX_3CR1^{bright} profile (**Fig. 4A–F**). The majority of ATMs was CX_3CR1^{bright}, both after birth and in adulthood (Fig. 4G). The so-called stage 4 YS Mϕs give rise to some tissue-resident Mϕs, and persist into adulthood [10, 11, 18, 40–43]. Furthermore, stage 4 YS-derived Mϕ progenitors can be identified by the early-onset expression of the chemokine receptor, CX_3CR1, which allows them to be tracked from embryonic day 9 onwards [10, 11, 18, 40–43].

We evaluated whether a homologous mechanism of BM-independent ATM development was operating in the mouse. We used a tamoxifen-inducible eGFP model to label CX_3CR1^+ stage 4 YS Mϕ progenitors at embryonic day 9 (Fig. 4H), and we analyzed the

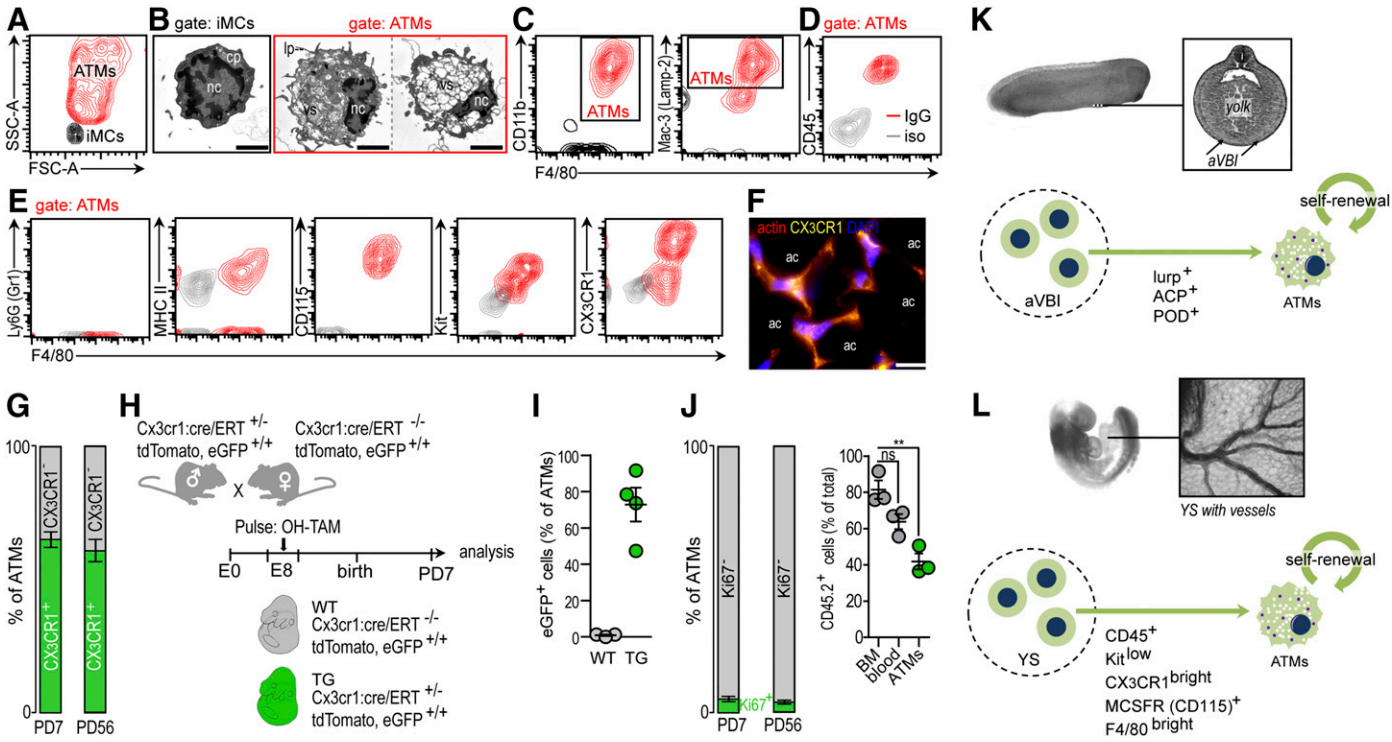

Figure 4. Homology of *Xenopus* and mouse ATM development. (A) FACS analysis of mouse SCs that were isolated from iWAT at postnatal day (PD) 7. Representative of 3 independent assays. Details of FACS analysis of ATMs have been described previously [19]. (B) TEM images of sorted cells of the iWAT stroma at PD7; also see Supplemental Fig. 4. Scale bar, 10 μm. (C) Identification of ATMs on the basis of CD11b, F4/80 antigen, and lysosomal protein Mac-3/Lamp-2 expression. Cells were isolated from iWAT at PD7. (D and E) Characterization of ATMs of the iWAT at PD7. (F) Immunohistochemistry against CX_3CR1 in iWAT at PD7. F-Actin was labeled with fluorescent phalloidin. (G) Percentage of CX_3CR1^+ ATMs in the iWAT at PD7 and PD56. (H) Scheme for labeling YS-derived Mϕs in the mouse. (I) Percentage of YS-derived (CX_3CR1-eGFP$^+$) ATMs in wild-type (WT) and transgenic (TG) iWAT at PD7 (Flow Repository accession number FR-FCM-ZYZW). (J) Percentage of Ki-67$^+$ ATMs in iWAT at PD7 and PD56, pooled data from 3 assays, and amount of CD45.2$^+$ leukocytes in BM and blood and epididymal WAT ATMs, 20 wk after BM transplantation (n = 3; Flow Repository accession number FR-FCM-ZYZW). (K and L) Scheme of the proposed homology of ATM development in *Xenopus* and mouse. FSC, forward scatter; iMC = immature myeloid cell, lp = lamellipoda, nc = nucleus, ns = non-significant, POD = peroxidase, SSC = side scatter, vs = vesicles. ** $P<0.01$, ANOVA with Dunnett's post-hoc test.

fat depots after birth. In mouse, BAT develops before birth [44]; therefore, we first examined the interscapular BAT 7 d after birth. Although we could not identify significant amounts of ATMs within BAT stroma (Supplemental Fig. 4), other myeloid cells, such as granulocytes and mast cells, were abundant (Supplemental Fig. 4). We next analyzed the inguinal fat depot (iWAT), which starts to expand at birth [44]. Of note, we found that the majority of ATMs was eGFP$^+$ at adulthood (Fig. 4I), which indicates that YS-derived ATMs persist in iWAT after birth. Moreover, we detected a similar amount of Ki-67$^+$ ATMs after birth and in adulthood (Fig. 4J), which demonstrates that ATMs proliferate locally. These findings demonstrate that mouse ATMs have a YS origin and retain the ability to proliferate. This is in accordance with our recent report that showed that ATMs are capable of self-renewal without the need for monocyte supply, and that proliferating ATMs in mouse express CX_3CR1 [45]. Furthermore, when we transplanted lineage-negative CD45.2$^+$ BM progenitors into lethally irradiated CD45.1$^+$ mice, we found that the majority of ATMs remained CD45.1$^+$ in the recipients (Fig. 4J).

Taken together, these data show that, similar to *X. laevis*, ATMs in the mouse have a BM-independent origin with the potential for self-renewal (Fig. 4K and L).

ATM development and activation in *X. laevis* is controlled by gpr147

Recent findings suggest that M2-activating cytokines allow for Mϕ self-renewal [46]; however, it is unknown whether M2 Mϕ activation occurs in vertebrates other than mammals. We thus sought to define whether *Xenopus* ATMs can polarize toward an M2-equivalent activation state as well as whether this can increase ATM proliferation. Under physiologic conditions, M2 ATM activation is maintained by various tissue factors in mammals, such as neurohormonal signals of fat metabolism [47]. While searching for hormone receptors that have abundant transcription in the *Xenopus* fat body, we identified *gpr147* as being specifically and highly expressed in WAT stroma of adult *Xenopus* (**Fig. 5A**). *Xenopus gpr147* encodes a putative GPCR, which is a homolog of the mammalian NPFF receptor; thus, *gpr147* is also called *npffr1*. The ligand for NPFF receptors, NPFF, is an evolutionarily conserved neuropeptide of deuterostomes [48] that has been shown to inhibit adipogenesis [49] and that has a plausible role in Mϕ activation in mammals [50]. Indeed, neuropeptides have an impact on immune cell functions in *Xenopus* [51] and Mϕ activation in mammals [52]. Given this information, we analyzed the effect of gpr147 on *Xenopus* ATM development. When we ablated *gpr147* in *Xenopus*, the first (F0)

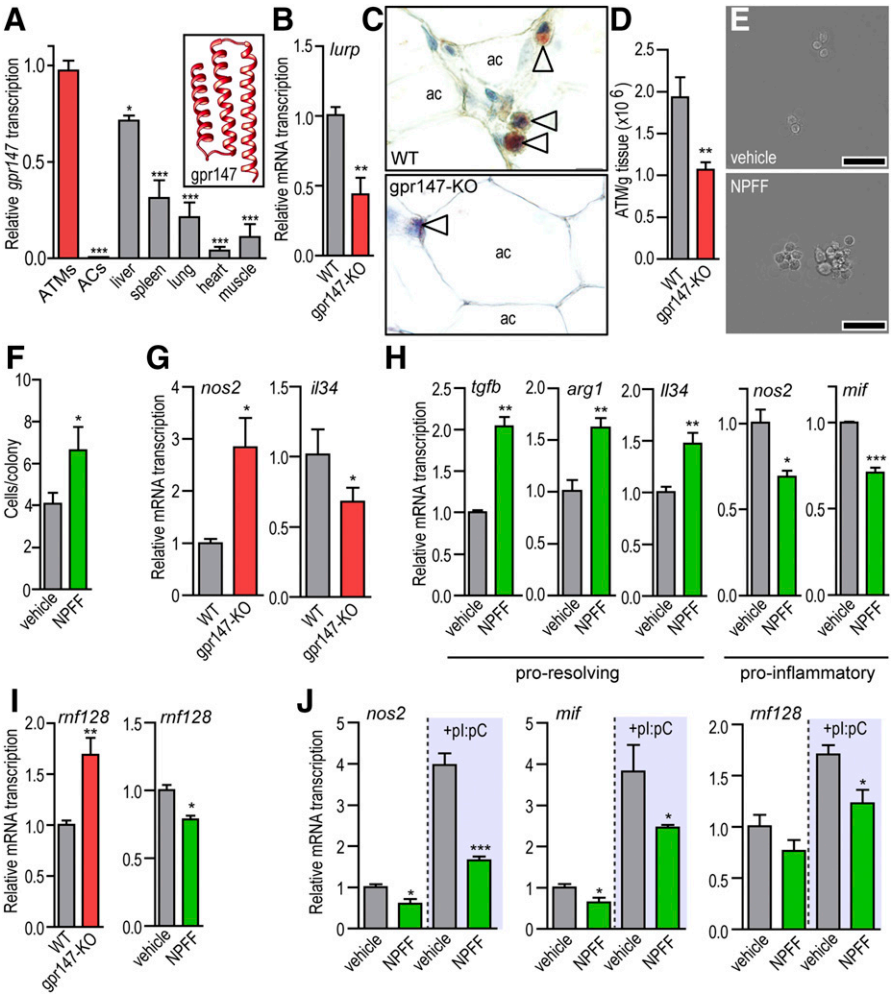

Figure 5. Control of ATM number and activation state by gpr147 and NPFF. (A) Relative transcription of *gpr147* mRNA in ATMs, adipocytes (ACs), and various tissues ($n = 4$). Transcript levels are normalized to ATMs. Insert shows predicted primary structure of *Xenopus* gpr147 using LOMETS structure prediction software [84]. (B) Transcription of *lurp* in wild-type (WT) and gpr147-KO fat body ($n = 5$). (C) ACP$^+$ cells (arrowhead) in fat body of WT and gpr147-KO adult frog. Scale bar, 50 μm. (D) Number of ATMs that were isolated from WT and gpr147-KO fat bodies of adult frogs ($n = 5$). (E) Representative images of SCs of a WT frog cultured in soft agar and treated with vehicle or 0.5 nM NPFF. Colonies were photographed at day 3 of treatment. (F) Size of vehicle- or NPFF-treated colonies ($n > 80$ each assay), pooled data of 3 assays. (G) Relative transcription of Mϕ activation genes in ATMs of WT and gpr147-KO frogs ($n = 5$). (H) *Xenopus* ATMs were treated with vehicle or 1 nM NPFF for 1 h in vitro and relative transcription of Mϕ activation genes was measured ($n = 3$). (I) Relative transcription of *rnf128* in WT and npffr1-KO ATMs ($n = 5$), and in ATMs treated in vitro with vehicle or 1 nM NPFF for 1 h ($n = 3$). (J) Relative transcription of Mϕ activation genes in ATMs of in vitro cultured *Xenopus* ATMs, treated with vehicle, 1 nM NPFF, pI:pC, or combination of pI:pC and NPFF for 4 h ($n = 3$). ac = adipocyte. $^*P < 0.05$; $^{**}P < 0.01$; $^{***}P < 0.001$, Student's t test (B–I), or 1-way ANOVA with Dunnett's post hoc test (A and J).

generation gpr147-KO animals presented a reduction in *lurp* transcription in WAT concomitant with a reduction in ATM content (Fig. 5B–D).

To test whether NPFF has an impact on *Xenopus* ATM content and activation, we treated ATMs with NPFF (1 nM) in vitro and found that NPFF-treated ATMs formed larger colonies in soft agar than did vehicle-treated ATMs (Fig. 5E and F). Moreover, when gpr147-KO ATMs were compared with wild-type ATMs, the level of expression of *nos2* and *il34* (encoding IL-34; IL-34) was significantly higher and lower, respectively, in gpr147-KO cells (Fig. 5G). Furthermore, NPFF-treated wild-type ATMs displayed increased transcription of the proresolving and profibrotic genes, *tgfb* and *arg1* (arginase-1) (Fig. 5H), both of which are hallmarks of M2 activation in mammalian Mϕs [47]. In nonmammalian vertebrates, arginase-1 and TGF-β are associated with tissue healing and the resolution of inflammation [47], which points to a possible role for NPFF in M2 activation in *Xenopus* ATMs. In addition, administration of NPFF increased the transcription of *il34* (Fig. 5H). It has been shown recently that *Xenopus* IL-34 induces a unique activation state of *Xenopus* Mϕs that is characterized by prominent *arg1* expression [53]. NPFF also suppressed the expression of the inflammatory genes, *nos2* and *mif* (Fig. 5H). In murine Mϕs, the M1 activation state is typified by *NOS2* expression and NO synthesis, whereas M2 activation is characterized by increased arginase-1 expression and the abolishment of NO synthesis [47]. As a homolog of this model, our data support the notion that pI:pC- or LPS-stimulated *Xenopus* Mϕs can be assigned as M1-Mϕs, and NPFF-treated Mϕs as M2-Mϕs. Deficiency for gpr147 increased the transcription of *rnf128*, whereas the opposite effect was observed with NPFF treatment (Fig. 5I). *Xenopus rnf128* is a homolog of the mammalian *Rnf128* or *Grail*, which encodes an E3 ubiquitin ligase that increases the proteasomal degradation of STAT6, the major signal transducer of M2 activation in mammals [54]. NPFF also inhibited pI:pC-induced transcriptional changes in ATMs (Fig. 5J).

It is known that NPFF is expressed in the amphibian brain [55]. In addition, we screened for NPFF expression in endocrine organs and found that only the pancreas had a notable NPFF content. Accordingly, NPFF-like immunoreactivity was present in endocrine cells of the pancreas, which were scattered in the exocrine parenchyma (Supplemental Fig. 5). The source of NPFF may thus be either the CNS or pancreatic endocrine cells.

DISCUSSION

ATMs have a key metabolic impact in mice and primates [2]; however, an evolutionary understanding of their equivalents and developmental origin is lacking. We have previously shown that ATMs are present in all relevant taxa of mammals [19]. Whereas the majority of studies with ATMs is centered on murine models of human obesity, some recent studies confirm that ATMs have a general metabolic and endocrine function in mammals [19, 56, 57]. In the present study, we show that ATMs are present in amphibian (*X. laevis* and *A. mexicanum*) WAT, which suggests that they are evolutionarily conserved constituents of WAT immune cell population in vertebrates.

Both amphibian and mammalian innate immune systems use Mϕs as a first line of defense against cellular and viral pathogens [16, 17, 32]; however, several key mechanisms remain to be defined in the development and function of the amphibian immune system [32]. Indeed, whereas the immune system of *Xenopus* is the most comprehensively studied outside mammals and chicken [32], the functions and the development of *Xenopus* tissue-resident Mϕs are relatively unknown. Mϕs are key for tissue regeneration in mammals [58], and studies using the axolotl, *A. mexicanum*, show that Mϕs are also crucial for tissue healing in this highly regenerative species [59–61]. However, the axolotl hematopoietic system has only recently been explored [38], and information on tissue-resident Mϕs in *Ambystoma* remains scarce in the literature [62–65]. Whereas some studies have shown that the amphibian liver contains phagocytosing Mϕs, which may be the equivalent of mammalian Kupffer cells [14, 66], these Mϕs synthesize and degrade melanin and are therefore different than Kupffer cells [14, 63]. Phagocytosing astrocytes and microglia are also present in amphibians and have roles in myelin remodeling and nerve injury regeneration [67, 68]. Moreover, bone resorbing cells in amphibians are thought to be homologs of mammalian osteoclasts [69] or odontoclasts [70]. It remains to be established whether amphibians have the equivalents of mammalian-type cardiac and intimal Mϕs and other types of tissue-resident Mϕs. Indeed, it has been shown that amphibians lack the specialized populations of leukocytes in tissues as well as lymph nodes, tonsils, and Peyer-plaques within mucosal layers [32, 71]. Our study identifies a novel accumulation site of leukocytes in the periphery and shows that WAT hosts a leukocyte niche that is formed by lymphocytes and ATMs. To our knowledge, this is the first study to demonstrate the existence of ATMs in nonmammalian vertebrates.

X. laevis and *A. mexicanum* are important model organisms in comparative studies of immunity, development, and regeneration [32, 72, 73], and it is therefore interesting that both species harbor ATMs in their fat depots. Moreover, *A. mexicanum* is a critically endangered species [74], and data on axolotl physiology, therefore, have high value for research. The evolutionary and genetic distance of amphibians from mammals allows for the recognition of those features of the immune system that are resistant to evolutionary change. In human and mouse, accumulation of ATMs was initially observed in a disease context and was considered a pathologic consequence of obesity [1, 2]. Nevertheless, our present and previous findings [19] show that the association of WAT and leukocytes, specifically ATMs, is a conserved trait of vertebrates. Although WAT is not exposed to the environment, blood circulation from the intestine can deliver pathogen-associated signals to WAT, which can elicit an innate immune response of ATMs. The close association of *Xenopus* ATMs with lymphocytes makes communication between these cells feasible and may be the evolutionary root of mammalian AT immune function.

Whereas Mϕs were traditionally viewed as terminally differentiated monocytes that lacked the capacity for proliferation and self-renewal [75], recent data challenge this view. It has been shown that monocyte recruitment to tissues is not the only possible source of tissue Mϕs. Indeed, microglia, liver Kupffer cells, and arterial and cardiac Mϕs have been shown to develop

without monocyte intermediates [11, 18]. Kupffer cells are replenished by a locally proliferating Mϕ progenitor pool [9], and microglia and arterial and cardiac Mϕs originate, at least in part, with self-renewing Mϕs of the embryonic YS [10, 18]. These findings suggest that tissue-resident Mϕs can locally proliferate [9], thereby allowing the replenishment of the tissue-specific Mϕ pool. Whereas the ontogeny of the majority of tissue-resident Mϕs has been explored in mammals, information on the origin of ATMs is lacking [2]. In obesity, ATMs are derived from circulating monocytes [7], but can also be produced by the local proliferation of ATMs [6]. Indeed, we have shown recently that ATMs can self-renew in lean AT in mouse [45]. ATM-specific delivery of anti-inflammatory drugs is a potential therapeutic approach for the targeted resolution of AT inflammation without inducing an unwanted general immunosuppression. The lack of information on the origin of ATMs [2], however, impedes the development of tools that can selectively target ATMs. Comparative studies, such as ours, are therefore important to better understand the developmental program of ATMs. In the present study, we show that *Xenopus* ATMs are derived from myeloid cell progenitors of aVBI and populate the developing AT before the establishment of the BM.

The developmental origin of tissue Mϕs in amphibians has been poorly investigated [34, 76]. Because the *Xenopus* embryo is exposed to the environment, its innate immune system develops rapidly and Mϕ progenitors appear 22–23 h postfertilization [32]. They invade peripheral tissues before the onset of the circulatory system [77] and exhibit *lurp* expression [34]. A recent study has described lurp$^-$ Mϕs in *Xenopus* [73], which may develop from a yet undefined myeloid lineage. As we show herein, ATMs express *lurp*, which indicates that they originate from aVBI progenitors. ATMs are present throughout the larval stage, metamorphosis, and adulthood, despite the distinct hematopoietic organs of these developmental stages. This indicates that ATM number is not affected by the change in the site of hematopoiesis or by the remodeling and down-regulation of immune function that normally occurs in metamorphosis [32]. This may be a consequence of the ability of ATMs to proliferate locally and, therefore, to replenish the ATM pool without the need for a hematopoietic organ. ATMs were also detected in the axolotl, *Ambystoma*, which lacks BM myeloid progenitors, further confirming that early larval hematopoiesis is sufficient to generate ATM progenitors and that ATMs can develop in species that lack BM hematopoiesis. However, the hematopoietic potential of the fat body is limited, as shown by the lack of erythropoiesis from fat body SCs and the low number of *scl*-expressing cells in AT stroma. We also show that ATM number and activation state is controlled by a neuropeptide in *Xenopus*. This further confirms that ATM development is a controlled physiologic process, rather than a passive and uncontrolled accumulation of Mϕs, as is currently considered [2].

We found that YS, the mammalian equivalent of aVBI, contributes to the ATM pool in mouse. A BM contribution to the generation of ATMs has been documented in obese mice [21], and BM-derived progenitors can give rise to phagocytic cells, which resemble adipocyte morphology but express Mϕ markers [78]. Of interest, whole-body irradiation followed by BM transplantation impedes the expansion of AT in genetically obese (*ob/ob*) mice and reduces AT transcription of *Mcp1*. These effects are thought to reduce monocyte recruitment to AT, thereby decreasing ATM number [79]; however, ATM content is not decreased after BM transplantation in *ob/ob* mice [79]. Moreover, ATM-associated metabolic effects of some nuclear receptors are not transmitted with BM transplantation [80]. These observations may be understood as signs of the existence of the BM-independent maintenance of ATM content. We also show in our study that BM can contribute to ATM replenishment after BM transplantation; however, BM-derived ATMs represent the minority of ATM content in mouse. Overall, our present findings, together with a recent study by us [45], establish the existence of a BM-independent replenishment of ATMs. We also show that the majority of ATMs have a YS origin in lean AT in mouse. Of importance, the prenatal development of ATM progenitors raises the possibility that maternal factors can have an impact on ATM number and activation state. Currently, much attention is paid to the effect of the prenatal environment on the risk for inflammatory diseases and metabolism in adulthood [81]. Maternal nutrition, inflammatory status, infections, and bioactive factors of the maternal blood can all have late-acting effects on immunity and metabolism [81]. Mϕ number and activation state are influenced by nutrition and by inflammatory mediators and bioactive factors, such as hormones and vitamins. It is feasible that these factors are also operative in the prenatal environment, though there are significant gaps in our understanding of prenatal Mϕ functions [82, 83]. As the *Xenopus* embryo develops externally, development of amphibian ATMs occurs without maternal influence, which makes *Xenopus* a tractable model system of ATM development via exposure to various inflammatory signals, hormones, and other bioactive factors.

Use of *Xenopus* as a model of ATM development has an additional advantage over mouse models because myeloid precursors are anatomically separated from erythroid and lymphoid progenitors in the early tailbud embryo [34, 77]. Although appropriate markers to distinguish the hematopoietic lineages in *Xenopus* by FACS analysis are lacking, this anatomic separation allows for the targeted manipulation of the early myeloid lineage and the identification of determinants of ATM development, which can lead to specific approaches that target ATM development without adverse off-target effects on other tissue Mϕs.

In summary, our study shows that the evolutionary history of WAT is shared with ATMs. As a result of the conservation of fundamental mechanisms of immunity between amphibians and mammals, exploring the features of amphibian ATM development will not only enhance the understanding of the amphibian immune response, per se, but will also aid in the understanding of the impact of ATM development on organ homeostasis and metabolism.

AUTHORSHIP

S.F.H.W., A.N., A.C.H., G.A., M.P. carried out experiments, S.S., M.G. provided resources, and T.R. conceived the project and wrote the article.

ACKNOWLEDGMENTS

This study was supported by the European Commission Horizon 2020 Research and Innovation Program, Marie-Curie-Skłodowska Individual Fellowship (655598, to T.R.), the German Research Fund (Deutsche Forschungsgemeinschaft) (RO 4856/1-1 to T.R.), the German Academic Exchange Service (Deutscher Akademischer Austauschdienst) (to S.F.H.W.), and the Department of Comparative Molecular Endocrinology (Director, Prof. Dr. Jan Tuckermann). Work at the European *Xenopus* Resource Centre was funded by the Wellcome Trust (101480Z to M.G.). The authors thank the laboratory of Prof. Dr. Michael Kühl (University of Ulm) for providing *X. laevis* tissues, the laboratory of Prof. Dr. Hartmut Geiger (Gina Moira Marka, Katharina Senger and Desirée Schütz, University of Ulm), for providing tissues of CD45.1/CD45.2 chimeric mice, Susanne Schmidt for her technical help, Dreamstime Stock Photography for providing the illustration of an adult *A. mexicanum* shown in Fig. 3F, Dr. Ricardo Costa for valuable discussion, and Dr. Kenneth McCreath for critical reading of the manuscript.

DISCLOSURES

The authors declare no conflicts of interest.

REFERENCES

1. Rosen, E. D., Spiegelman, B. M. (2014) What we talk about when we talk about fat. *Cell* **156,** 20–44.
2. Boutens, L., Stienstra, R. (2016) Adipose tissue macrophages: going off track during obesity. *Diabetologia* **59,** 879–894.
3. Osborn, O., Olefsky, J. M. (2012) The cellular and signaling networks linking the immune system and metabolism in disease. *Nat. Med.* **18,** 363–374.
4. Qiu, Y., Nguyen, K. D., Odegaard, J. I., Cui, X., Tian, X., Locksley, R. M., Palmiter, R. D., Chawla, A. (2014) Eosinophils and type 2 cytokine signaling in macrophages orchestrate development of functional beige fat. *Cell* **157,** 1292–1308.
5. Lawrence, T., Natoli, G. (2011) Transcriptional regulation of macrophage polarization: enabling diversity with identity. *Nat. Rev. Immunol.* **11,** 750–761.
6. Amano, S. U., Cohen, J. L., Vangala, P., Tencerova, M., Nicoloro, S. M., Yawe, J. C., Shen, Y., Czech, M. P., Aouadi, M. (2014) Local proliferation of macrophages contributes to obesity-associated adipose tissue inflammation. *Cell Metab.* **19,** 162–171.
7. Lumeng, C. N., Bodzin, J. L., Saltiel, A. R. (2007) Obesity induces a phenotypic switch in adipose tissue macrophage polarization. *J. Clin. Invest.* **117,** 175–184.
8. Lee, B. C., Lee, J. (2014) Cellular and molecular players in adipose tissue inflammation in the development of obesity-induced insulin resistance. *Biochim. Biophys. Acta* **1842,** 446–462.
9. Scott, C. L., Zheng, F., De Baetselier, P., Martens, L., Saeys, Y., De Prijck, S., Lippens, S., Abels, C., Schoonooghe, S., Raes, G., Devoogdt, N., Lambrecht, B. N., Beschin, A., Guilliams, M. (2016) Bone marrow-derived monocytes give rise to self-renewing and fully differentiated Kupffer cells. *Nat. Commun.* **7,** 10321.
10. Ensan, S., Li, A., Besla, R., Degousee, N., Cosme, J., Roufaiel, M., Shikatani, E. A., El-Maklizi, M., Williams, J. W., Robins, L., Li, C., Lewis, B., Yun, T. J., Lee, J. S., Wieghofer, P., Khattar, R., Farrokhi, K., Byrne, J., Ouzounian, M., Zavitz, C. C., Levy, G. A., Bauer, C. M., Libby, P., Husain, M., Swirski, F. K., Cheong, C., Prinz, M., Hilgendorf, I., Randolph, G. J., Epelman, S., Gramolini, A. O., Cybulsky, M. I., Rubin, B. B., Robbins, C. S. (2016) Self-renewing resident arterial macrophages arise from embryonic CX3CR1^{+} precursors and circulating monocytes immediately after birth. *Nat. Immunol.* **17,** 159–168.
11. Molawi, K., Wolf, Y., Kandalla, P. K., Favret, J., Hagemeyer, N., Frenzel, K., Pinto, A. R., Klapproth, K., Henri, S., Malissen, B., Rodewald, H. R., Rosenthal, N. A., Bajenoff, M., Prinz, M., Jung, S., Sieweke, M. H. (2014) Progressive replacement of embryo-derived cardiac macrophages with age. *J. Exp. Med.* **211,** 2151–2158.
12. Soucie, E. L., Weng, Z., Geirsdóttir, L., Molawi, K., Maurizio, J., Fenouil, R., Mossadegh-Keller, N., Gimenez, G., VanHille, L., Beniazza, M., Favret, J., Berruyer, C., Perrin, P., Hacohen, N., Andrau, J. C., Ferrier, P., Dubreuil, P., Sidow, A., Sieweke, M. H. (2016) Lineage-specific enhancers activate self-renewal genes in macrophages and embryonic stem cells. *Science* **351,** aad5510.
13. Tinsley, R. (2010) Amphibians, with special reference to *Xenopus*. In *The UFAW Handbook on the Care and Management of Laboratory and Other Research Animals*, 8th Ed. (R. C. Hubrecht, J. Kirkwoo, eds.), Wiley-Blackwell, Oxford, DOI: 10.1002/9781444318777.ch48.
14. Faber, J., Nieuwkoop, P. D. (1967) *Normal Table of* Xenopus laevis *(Daudin): A Systematical and Chronological Survey of the Development from the Fertilized Egg Till the End of Metamorphosis*, North-Holland, Amsterdam.
15. Schultschik, G., Große, W.-R. (2013) *Threatened Newts and Salamanders of the World - Captive Care Management*, DGHT, Mannheim, Germany.
16. Guille, M. 1999. *Molecular Methods in Developmental Biology:* Xenopus *and* Zebrafish. Humana Press, New York.
17. Nakayama, T., Blitz, I. L., Fish, M. B., Odeleye, A. O., Manohar, S., Cho, K. W., Grainger, R. M. (2014) Cas9-based genome editing in *Xenopus tropicalis*. *Methods Enzymol.* **546,** 355–375.
18. Epelman, S., Lavine, K. J., Beaudin, A. E., Sojka, D. K., Carrero, J. A., Calderon, B., Brija, T., Gautier, E. L., Ivanov, S., Satpathy, A. T., Schilling, J. D., Schwendener, R., Sergin, I., Razani, B., Forsberg, E. C., Yokoyama, W. M., Unanue, E. R., Colonna, M., Randolph, G. J., Mann, D. L. (2014) Embryonic and adult-derived resident cardiac macrophages are maintained through distinct mechanisms at steady state and during inflammation. *Immunity* **40,** 91–104.
19. Ampem, G., Azegrouz, H., Bacsadi, Á., Balogh, L., Schmidt, S., Thuróczy, J., Röszer, T. (2016) Adipose tissue macrophages in non-rodent mammals: a comparative study. *Cell Tissue Res.* **363,** 461–478.
20. Silveira, S. R., Hadler, W. A. (1978) Catalases and peroxidases histochemical detection; techniques suitable to discriminate these enzymes. *Acta Histochem.* **63,** 1–10.
21. Weisberg, S. P., McCann, D., Desai, M., Rosenbaum, M., Leibel, R. L., Ferrante, A. W., Jr. (2003) Obesity is associated with macrophage accumulation in adipose tissue. *J. Clin. Invest.* **112,** 1796–1808.
22. Nogawa-Kosaka, N., Sugai, T., Nagasawa, K., Tanizaki, Y., Meguro, M., Aizawa, Y., Maekawa, S., Adachi, M., Kuroki, R., Kato, T. (2011) Identification of erythroid progenitors induced by erythropoietic activity in *Xenopus laevis*. *J. Exp. Biol.* **214,** 921–927.
23. Röszer, T., Menéndez-Gutiérrez, M. P., Lefterova, M. I., Alameda, D., Núñez, V., Lazar, M. A., Fischer, T., Ricote, M. (2011) Autoimmune kidney disease and impaired engulfment of apoptotic cells in mice with macrophage peroxisome proliferator-activated receptor gamma or retinoid X receptor alpha deficiency. *J. Immunol.* **186,** 621–631.
24. Ottaviani, E., Malagoli, D., Franceschi, C. (2011) The evolution of the adipose tissue: a neglected enigma. *Gen. Comp. Endocrinol.* **174,** 1–4.
25. Fenoglio, C., Boncompagni, E., Fasola, M., Gandini, C., Comizzoli, S., Milanesi, G., Barni, S. (2005) Effects of environmental pollution on the liver parenchymal cells and Kupffer-melanomacrophagic cells of the frog *Rana esculenta*. *Ecotoxicol. Environ. Saf.* **60,** 259–268.
26. Gallone, A., Guida, G., Maida, I., Cicero, R. (2002) Spleen and liver pigmented macrophages of *Rana esculenta* L. A new melanogenic system? *Pigment Cell Res.* **15,** 32–40.
27. Morales, H. D., Abramowitz, L., Gertz, J., Sowa, J., Vogel, A., Robert, J. (2010) Innate immune responses and permissiveness to ranavirus infection of peritoneal leukocytes in the frog *Xenopus laevis*. *J. Virol.* **84,** 4912–4922.
28. Grayfer, L., Robert, J. (2016) Amphibian macrophage development and antiviral defenses. *Dev. Comp. Immunol.* **58,** 60–67.
29. Grayfer, L., De Jesús Andino, F., Robert, J. (2015) Prominent amphibian (*Xenopus laevis*) tadpole type III interferon response to the frog virus 3 ranavirus. *J. Virol.* **89,** 5072–5082.
30. Qi, Z. T., Nie, P. (2008) Comparative study and expression analysis of the interferon gamma gene locus cytokines in *Xenopus tropicalis*. *Immunogenetics* **60,** 699–710.
31. Tomiyama, S., Nakamachi, T., Uchiyama, M., Matsuda, K., Konno, N. (2015) Urotensin II upregulates migration and cytokine gene expression in leukocytes of the African clawed frog, *Xenopus laevis*. *Gen. Comp. Endocrinol.* **216,** 54–63.
32. Robert, J., Ohta, Y. (2009) Comparative and developmental study of the immune system in *Xenopus*. *Dev. Dyn.* **238,** 1249–1270.
33. Haase, J., Weyer, U., Immig, K., Klöting, N., Blüher, M., Eilers, J., Bechmann, I., Gericke, M. (2014) Local proliferation of macrophages in adipose tissue during obesity-induced inflammation. *Diabetologia* **57,** 562–571.
34. Smith, S. J., Kotecha, S., Towers, N., Latinkic, B. V., Mohun, T. J. (2002) XPOX2-peroxidase expression and the XLURP-1 promoter reveal the site of embryonic myeloid cell development in *Xenopus*. *Mech. Dev.* **117,** 173–186.
35. Ciau-Uitz, A., Pinheiro, P., Kirmizitas, A., Zuo, J., Patient, R. (2013) VEGFA-dependent and -independent pathways synergise to drive Scl expression and initiate programming of the blood stem cell lineage in *Xenopus*. *Development* **140,** 2632–2642.
36. Chen, X. D., Turpen, J. B. (1995) Intraembryonic origin of hepatic hematopoiesis in *Xenopus laevis*. *J. Immunol.* **154,** 2557–2567.

37. Yaparla, A., Wendel, E. S., Grayfer, L. (2016) The unique myelopoiesis strategy of the amphibian *Xenopus laevis*. *Dev. Comp. Immunol.* **63,** 136–143.
38. Lopez, D., Lin, L., Monaghan, J. R., Cogle, C. R., Bova, F. J., Maden, M., Scott, E. W. (2014) Mapping hematopoiesis in a fully regenerative vertebrate: the axolotl. *Blood* **124,** 1232–1241.
39. Balic, A., Garcia-Morales, C., Vervelde, L., Gilhooley, H., Sherman, A., Garceau, V., Gutowska, M. W., Burt, D. W., Kaiser, P., Hume, D. A., Sang, H. M. (2014) Visualisation of chicken macrophages using transgenic reporter genes: insights into the development of the avian macrophage lineage. *Development* **141,** 3255–3265.
40. Perdiguero, E. G., Klapproth, K., Schulz, C., Busch, K., Azzoni, E., Crozet, L., Garner, H., Trouillet, C., de Bruijn, M. F., Geissmann, F., Rodewald, H. R. (2015) Tissue-resident macrophages originate from yolk-sac-derived erythro-myeloid progenitors. *Nature* **518,** 547–551.
41. Schulz, C., Gomez Perdiguero, E., Chorro, L., Szabo-Rogers, H., Cagnard, N., Kierdorf, K., Prinz, M., Wu, B., Jacobsen, S. E., Pollard, J. W., Frampton, J., Liu, K. J., Geissmann, F. (2012) A lineage of myeloid cells independent of Myb and hematopoietic stem cells. *Science* **336,** 86–90.
42. Yona, S., Kim, K. W., Wolf, Y., Mildner, A., Varol, D., Breker, M., Strauss-Ayali, D., Viukov, S., Guilliams, M., Misharin, A., Hume, D. A., Perlman, H., Malissen, B., Zelzer, E., Jung, S. (2013) Fate mapping reveals origins and dynamics of monocytes and tissue macrophages under homeostasis. *Immunity* **38,** 79–91.
43. DeFalco, T., Bhattacharya, I., Williams, A. V., Sams, D. M., Capel, B. (2014) Yolk-sac-derived macrophages regulate fetal testis vascularization and morphogenesis. *Proc. Natl. Acad. Sci. USA* **111,** E2384–E2393.
44. Kozak, L. P. (2011) The genetics of brown adipocyte induction in white fat depots. *Front. Endocrinol. (Lausanne)* **2,** 64.
45. Waqas, S. F. H., Hoang, A. C., Lin, Y., Ampem, G., Azegrouz, H., Balogh, L., Thuróczy, J., Chen, J., Gerling, I. C., Nam, S., Lim, J., Martinez-Ibañez, J., Real, J. T., Paschke, S., Quillet, R., Ayachi, S., Simonin, F., Schneider, M., Brinkman, J., Lamming, D. W., Seroogy, C. M., Röszer, T. (2017) Neuropeptide FF increases M2 activation and self-renewal of adipose tissue macrophages. *J. Clin. Invest.* [Epub ahead of print]. doi: 10.1172/JC190152
46. Jenkins, S. J., Ruckerl, D., Cook, P. C., Jones, L. H., Finkelman, F. D., van Rooijen, N., MacDonald, A. S., Allen, J. E. (2011) Local macrophage proliferation, rather than recruitment from the blood, is a signature of TH2 inflammation. *Science* **332,** 1284–1288.
47. Röszer, T. (2015) Understanding the mysterious M2 macrophage through activation markers and effector mechanisms. *Mediators Inflamm.* **2015,** 1–16.
48. Elphick, M. R., Mirabeau, O. (2014) The evolution and variety of RFamide-type neuropeptides: insights from deuterostomian invertebrates. *Front. Endocrinol. (Lausanne)* **5,** 93.
49. Herrera-Herrera, M. L., Salazar-Olivo, L. A. (2008) RFamide neuropeptides inhibit murine and human adipose differentiation. *Biochem. Biophys. Res. Commun.* **377,** 29–34.
50. Sun, Y. L., Zhang, X. Y., Sun, T., He, N., Li, J. Y., Zhuang, Y., Zeng, Q., Yu, J., Fang, Q., Wang, R. (2013) The anti-inflammatory potential of neuropeptide FF in vitro and in vivo. *Peptides* **47,** 124–132.
51. Silva, A. B., Aw, D., Palmer, D. B. (2009) Neuropeptides and thymic hormones in the *Xenopus thymus*. *Front. Biosci. (Landmark Ed.)* **14,** 1990–2003.
52. Ganea, D., Delgado, M. (2001) Inhibitory neuropeptide receptors on macrophages. *Microbes Infect.* **3,** 141–147.
53. Grayfer, L., Robert, J. (2015) Distinct functional roles of amphibian (*Xenopus laevis*) colony-stimulating factor-1- and interleukin-34-derived macrophages. *J. Leukoc. Biol.* **98,** 641–649.
54. Sahoo, A., Alekseev, A., Obertas, L., Nurieva, R. (2014) Grail controls Th2 cell development by targeting STAT6 for degradation. *Nat. Commun.* **5,** 4732.
55. López, J. M., Moreno, N., Morona, R., Muñoz, M., González, A. (2006) Spatiotemporal sequence of appearance of NPFF-immunoreactive structures in the developing central nervous system of *Xenopus laevis*. *Peptides* **27,** 1036–1053.
56. Ramsay, T. G., Stoll, M. J., Blomberg, A., Caperna, T. J. (2016) Regulation of cytokine gene expression by orosomucoid in neonatal swine adipose tissue. *J. Anim. Sci. Biotechnol.* **7,** 25.
57. Westover, A. J., Johnston, K. A., Buffington, D. A., Humes, H. D. (2016) An immunomodulatory device improves insulin resistance in obese porcine model of metabolic syndrome. *J. Diabetes Res.* **2016,** 3486727.
58. Forbes, S. J., Rosenthal, N. (2014) Preparing the ground for tissue regeneration: from mechanism to therapy. *Nat. Med.* **20,** 857–869.
59. Godwin, J. W., Pinto, A. R., Rosenthal, N. A. (2013) Macrophages are required for adult salamander limb regeneration. *Proc. Natl. Acad. Sci. USA* **110,** 9415–9420.
60. Zammit, P. S., Clarke, J. D., Golding, J. P., Goodbrand, I. A., Tonge, D. A. (1993) Macrophage response during axonal regeneration in the axolotl central and peripheral nervous system. *Neuroscience* **54,** 781–789.
61. Jones, J. E., Corwin, J. T. (1996) Regeneration of sensory cells after laser ablation in the lateral line system: hair cell lineage and macrophage behavior revealed by time-lapse video microscopy. *J. Neurosci.* **16,** 649–662.
62. Takahama, H., Kinoshita, T., Sasaki, F. (1992) Structural and endocytotic differences of fibroblasts and macrophages in the tail fin of amphibian larvae during metamorphosis. *Arch. Histol. Cytol.* **55,** 437–448.
63. Sichel, G., Scalia, M., Mondio, F., Corsaro, C. (1997) The amphibian Kupffer cells build and demolish melanosomes: an ultrastructural point of view. *Pigment Cell Res.* **10,** 271–287.
64. Corsaro, C., Scalia, M., Leotta, N., Mondio, F., Sichel, G. (2000) Characterisation of Kupffer cells in some Amphibia. *J. Anat.* **196,** 249–261.
65. Scalia, M., Di Pietro, C., Poma, M., Ragusa, M., Sichel, G., Corsaro, C. (2004) The spleen pigment cells in some amphibia. *Pigment Cell Res.* **17,** 119–127.
66. Sichel, G., Scalia, M., Corsaro, C. (2002) Amphibia Kupffer cells. *Microsc. Res. Tech.* **57,** 477–490.
67. Kirkham, M., Berg, D. A., Simon, A. (2011) Microglia activation during neuroregeneration in the adult vertebrate brain. *Neurosci. Lett.* **497,** 11–16.
68. Mills, E. A., Davis, C. H., Bushong, E. A., Boassa, D., Kim, K. Y., Ellisman, M. H., Marsh-Armstrong, N. (2015) Astrocytes phagocytose focal dystrophies from shortening myelin segments in the optic nerve of *Xenopus laevis* at metamorphosis. *Proc. Natl. Acad. Sci. USA* **112,** 10509–10514.
69. Yaeger, J. A., Kraucunas, E. (1969) Fine structure of the resorptive cells in the teeth of frogs. *Anat. Rec.* **164,** 1–13.
70. Wistuba, J., Bolte, M., Clemen, G. (2000) The odontoclasts of *Ambystoma mexicanum*. *Ann. Anat.* **182,** 415–422.
71. Colombo, B. M., Scalvenzi, T., Benlamara, S., Pollet, N. (2015) Microbiota and mucosal immunity in amphibians. *Front. Immunol.* **6,** 111.
72. McCusker, C., Gardiner, D. M. (2011) The axolotl model for regeneration and aging research: a mini-review. *Gerontology* **57,** 565–571.
73. Paredes, R., Ishibashi, S., Borrill, R., Robert, J., Amaya, E. (2015) *Xenopus*: an in vivo model for imaging the inflammatory response following injury and bacterial infection. *Dev. Biol.* **408,** 213–228.
74. International Union for Conservation of Nature and Natural Resources. *Ambystoma mexicanum*. The IUCN Red List of Threatened Species. Available from http://www.iucnredlist.org/details/1095/0. Accessed November 11, 2008.
75. Chang, Z. L. (2009) Recent development of the mononuclear phagocyte system: in memory of Metchnikoff and Ehrlich on the 100th anniversary of the 1908 Nobel Prize in physiology or medicine. *Biol. Cell* **101,** 709–721.
76. Fischman, D. A., Hay, E. D. (1962) Origin of osteoclasts from mononuclear leucocytes in regenerating newt limbs. *Anat. Rec.* **143,** 329–337.
77. Costa, R. M., Soto, X., Chen, Y., Zorn, A. M., Amaya, E. (2008) spib is required for primitive myeloid development in Xenopus. *Blood* **112,** 2287–2296.
78. Koh, Y. J., Kang, S., Lee, H. J., Choi, T. S., Lee, H. S., Cho, C. H., Koh, G. Y. (2007) Bone marrow-derived circulating progenitor cells fail to transdifferentiate into adipocytes in adult adipose tissues in mice. *J. Clin. Invest.* **117,** 3684–3695.
79. Ablamunits, V., Weisberg, S. P., Lemieux, J. E., Combs, T. P., Klebanov, S. (2007) Reduced adiposity in ob/ob mice following total body irradiation and bone marrow transplantation. *Obesity (Silver Spring)* **15,** 1419–1429.
80. Marathe, C., Bradley, M. N., Hong, C., Chao, L., Wilpitz, D., Salazar, J., Tontonoz, P. (2009) Preserved glucose tolerance in high-fat-fed C57BL/6 mice transplanted with PPARgamma-/-, PPARdelta-/-, PPARgammadelta-/-, or LXRalphabeta-/- bone marrow. *J. Lipid Res.* **50,** 214–224.
81. Claycombe, K. J., Brissette, C. A., Ghribi, O. (2015) Epigenetics of inflammation, maternal infection, and nutrition. *J. Nutr.* **145,** 1109S–1115S.
82. Wang, H., He, M., Hou, Y., Chen, S., Zhang, X., Zhang, M., Ji, X. (2016) Role of decidual $CD14^+$ macrophages in the homeostasis of maternal-fetal interface and the differentiation capacity of the cells during pregnancy and parturition. *Placenta* **38,** 76–83.
83. Roger, T., Schneider, A., Weier, M., Sweep, F. C., Le Roy, D., Bernhagen, J., Calandra, T., Giannoni, E. (2016) High expression levels of macrophage migration inhibitory factor sustain the innate immune responses of neonates. *Proc. Natl. Acad. Sci. USA* **113,** E997–E1005.
84. Wu, S., Zhang, Y. (2007) LOMETS: a local meta-threading-server for protein structure prediction. *Nucleic Acids Res.* **35,** 3375–3382.

KEY WORDS:
fat body · yolk sac Mϕs · CX_3CR1 · neuropeptide FF